ELSEVIER

Journal of Alloys and Compounds 218 (1995) 244–254

Journal of ALLOYS AND COMPOUNDS

Structural stability of networks in main group intermetallics

Ulrich Häußermann, Reinhard Nesper *

Laboratory for Inorganic Chemistry, ETH-Zürich, Universitätstr. 6, CH-8092 Zürich, Switzerland

Received 8 June 1994; in final form 2 September 1994

Abstract

The relative stability of three-dimensional nets formed by gallium or aluminium in intermetallic phases has been investigated within the simple tight-binding Hückel model. In order to compare structures with different coordination numbers, the bond lengths of the nets have been changed according to the structural energy difference theorem. The structural stability as a function of the electron concentration per atom agrees well with the composition of the correspondent intermetallic compounds. The third and fourth moments of the density of states explain qualitatively the energy difference curves but are not sufficient to reproduce all the stability trends.

Keywords: Structural stability; Main group intermetallics; Tight-binding Hückel investigation; Method of moments

1. Introduction

Intermetallic phases formed between group 13 metallic elements (E13) (i.e. Al, Ga, In, Tl) and one or more of the more electropositive alkali or alkali earth metals show a rich variety of very often complex structures. In most cases this complexity originates in the substructure of the E13 component, where short distances between E13 atoms are typical. Although metallic conductivity is found for the majority of these compounds, covalent bonding plays a pivotal role for the substructures of the E13 elements. This induces a strong relationship between the geometrical structure and the valence electron concentration (VEC). The simple Zintl–Klemm concept, which is very successful for the interpretation of such relationships in semiconducting Zintl phases, is often at its limits for these intermetallic compounds. However, it is still reasonable to describe the E13 substructure as a polyanion and investigate the optimal VEC for the particular geometry of the substructure.

One may roughly distinguish between three classes of E13 substructures in the binary compounds: in the first class E13 atoms form frameworks of clusters, typical of alkali metal gallides [1], in the second class E13 atoms form networks apparently without clusters, occurring in alkali earth aluminides and gallides, and in the third class substructures consist of isolated clusters, as found in the recently reported alkali indides and thallides [2,3].

The first group has been examined theoretically by Burdett and Canadell [4]: when the deltahedral clusters are linked together, the electronic requirement can be understood by applying Wade's rules [5] for the cluster units and regarding the linkage either as two-electron–two-centre (2e2c) or 2e3c bonding. An electron-counting scheme for fused clusters, however, is far more complex and in some cases still not applicable. The fusion of clusters or cluster fragments reveal the transition to the open (but still electron-deficient) network structures corresponding to the second group. The relationship between geometrical structure and VEC is much more hidden in such structures. This is because the fragmentation and associated assignment of definite electron numbers for particular structure units are from an electronic point of view often ambiguous and not satisfactory.

For a theoretical investigation of electron-deficient network structures the method of moments [6] appears to be very useful. It allows the interpretation of structural trends without an orbital picture. Within the second group of substructures an increase in VEC induces the transition from electron-deficient networks to those obeying the octet rule (VEC > 4). The latter structures are sometimes classified as valency compounds [7].

In this paper we have examined the relationship between geometrical structure and VEC along this transition. At the beginning we introduce a number of three-dimensional (3D) nets formed by E13 atoms and stress the remarkable geometrical relations between them. Then we outline the calculation procedure for

* Corresponding author.

SSDI 0925-8388(94)01388-8

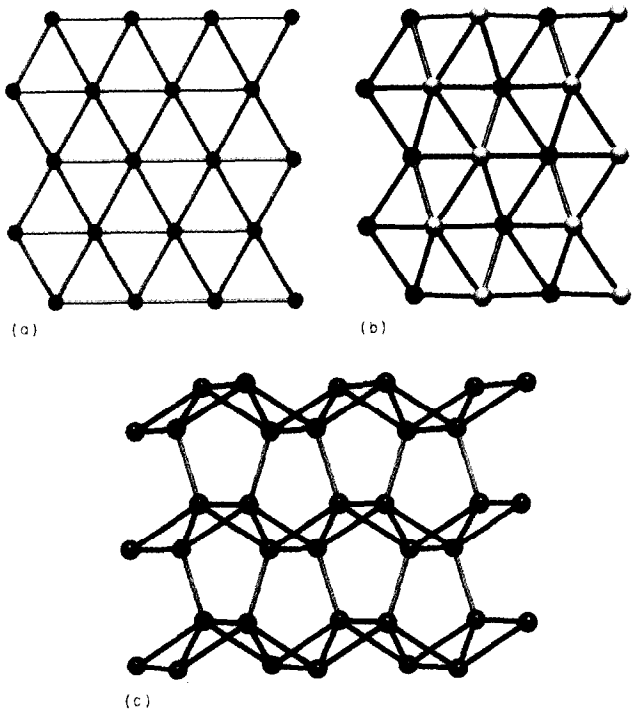

Fig. 1. (a) The triangular 3^6 net. (b) The corrugated 3^6 net in the α-Ga structure. (c) Stacking of the corrugated 3^6 nets (black) via short bonds (grey) leads to the α-Ga structure.

the determination of the structural stability within the tight-binding (TB) theory and present the obtained energy difference curves as a function of VEC. Finally we try to correlate the structural trends with the behaviour of the third and fourth moments of the density of states [8].

Fig. 1(a) shows the triangular 3^6 net formed by closest packing of equivalent spheres. It is the building block of the close-packed metallic structure types, in the simplest cases f.c.c. and h.c.p. Considering only sp-bonded systems, these structures are found to be stable for fairly low VEC.

The more electron-rich metal gallium adopts the α-Ga structure [9]. The main structural unit is a corrugated 3^6 net (Fig. 1(b)) which can be derived from the plane net (Fig. 1(a)) by a simple distortion. If the dark spheres of Fig. 1(b) are lowered below the paper plane and the light ones are raised by the same amount, the puckering is controlled by only one parameter. Lee et al. [10] were able to show that the degree of puckering as a function of band filling agrees exactly with the electron concentration of Ga. The corrugated layers are connected by the shortest bonds in the structure (Fig. 1(c)). An attractive interpretation of the α-Ga structure is to relate it to the boron structure [11]. The short distances in the α-Ga structure then correspond to the terminal bonds of the B_{12} icosahedra and can be regarded as 2e2c bonds. The electronic states related to the buckled layers are delocalized and are responsible for the metallic behaviour [12]. The latter corresponds to the multicentre bonding in the framework of the B_{12} icosahedra. In conclusion, the

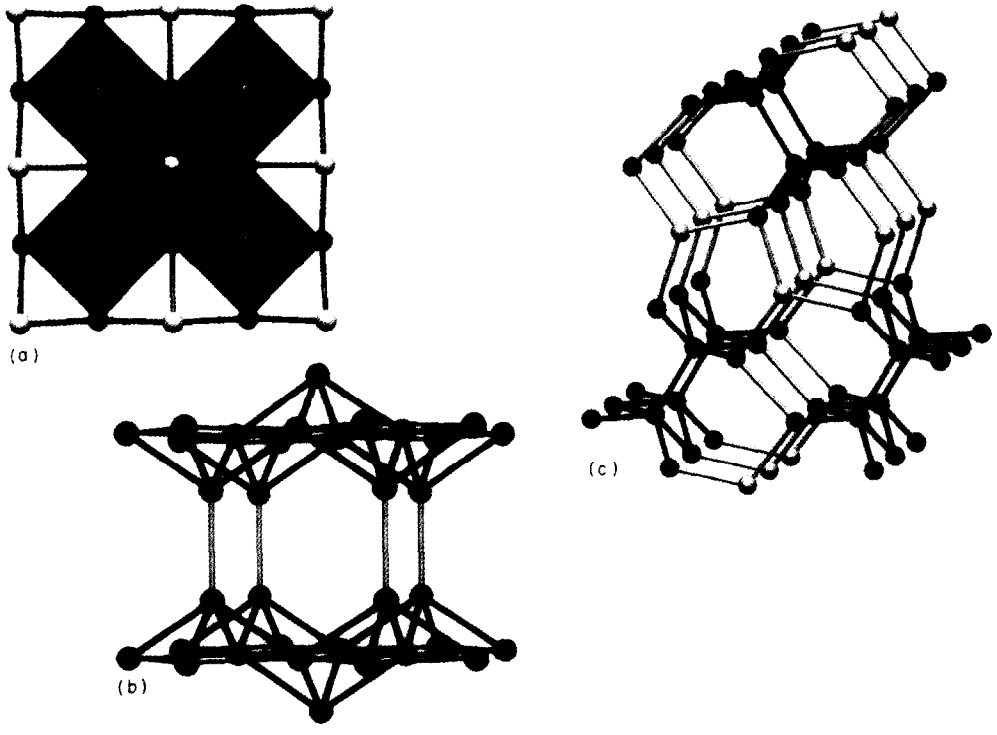

Fig. 2. (a) The 2D layer of pyramids formed by Al atoms in $BaAl_4$. (b) Stacking of the 2D layers (black) in the Al network of $BaAl_4$. (c) The Ga network in the $MgGa_2$ structure. Chains of the $BaAl_4$ structure (black) are connected directly or by trigonal-planar-coordinated Ga atoms.

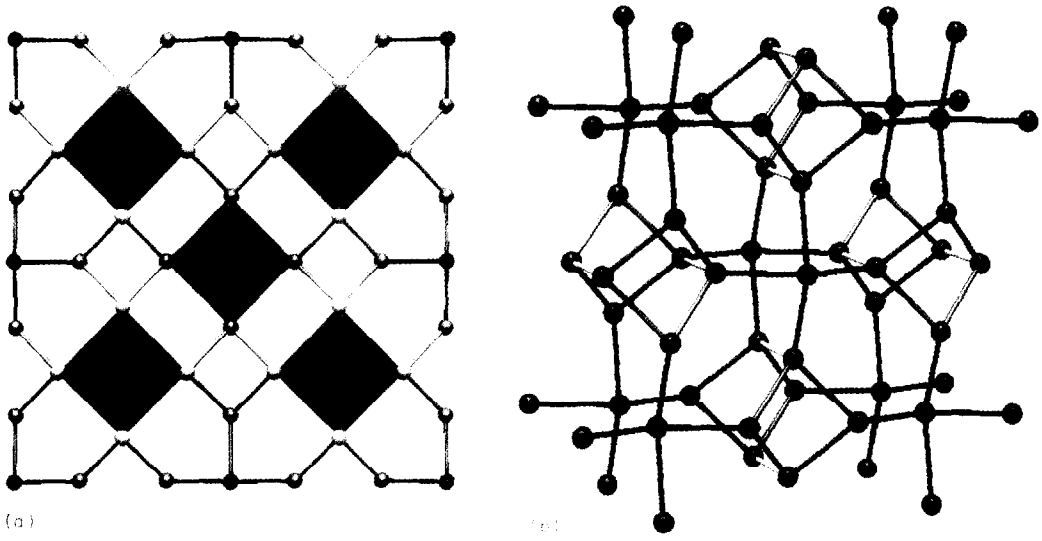

Fig. 3. (a) The 2D building block of the Ga network in Mg_2Ga_5. It consists of pyramids which are linked by bonds between the basal atoms, in contrast with the 2D layer in the $BaAl_4$ structure where the pyramids are condensed. (b) Stacking of the 2D units in the Ga network in Mg_2Ga_5.

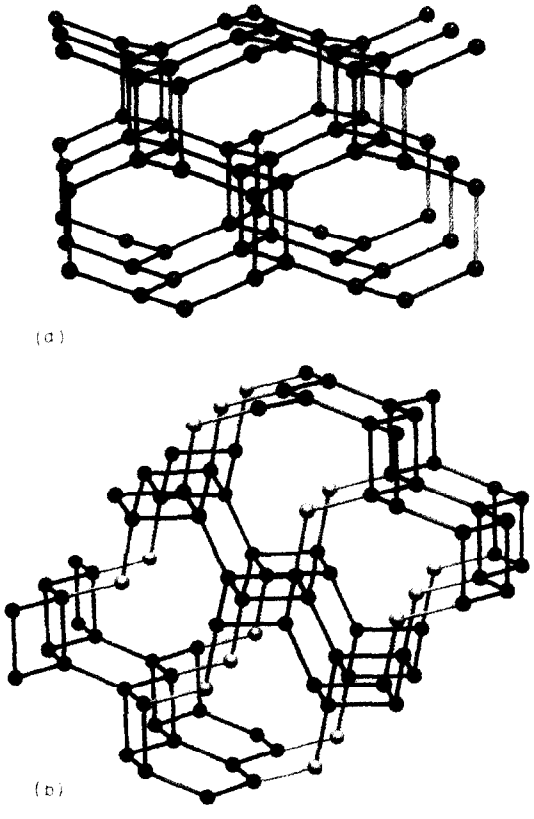

Fig. 4. (a) The Al network in $SrAl_2$. Longer bonds (grey) connect the slightly puckered layers of six-membered rings (black). (b) The Ga network in Ca_3Ga_5. 2D pieces of the $SrAl_2$ structure (black) are linked via two-bonded Ga atoms.

α-Ga structure shows a transition from the close-packed metals to a valency compound.

Fig. 2(a) shows the building unit of the Al substructure in $BaAl_4$ [13]. One kind of Al atoms (black spheres in Fig. 2(a)), which are called basal aluminium atoms, form a quadratic net with long non-bonding distances. The squares are capped alternately above (white spheres in Fig. 2(a)) and below (grey spheres in Fig. 2(a)) with the other kind of Al atoms, the apical ones. This capping leads to a layer of pyramids. The final network of the Al substructure results when these layers are connected by bonds between apical atoms which are located on top of each other (Fig. 2(b)). $SrAl_4$, $BaGa_4$ and $SrGa_4$ also crystallize in this structure type. Theoretical investigations [14] suggested a 2e2c bond between the layers connecting apical atoms and multicentre electron-deficient bonding in the pyramids between one apical and four basal atoms.

The Ga substructure of $MgGa_2$ [15] (Fig. 2(c)) is strikingly similar to the Al substructure in $BaAl_4$: chains of top-connected pyramids are linked together either directly or via trigonal-planar-coordinated Ga atoms.

In the Ga substructure of Mg_2Ga_5 [16] the pyramid is again the central structural unit. Fig. 3(a) shows the pyramid-containing layer. In contrast with the $BaAl_4$ structure, the apical atoms (black spheres in Fig. 3(a)) have about the same height and the basal Ga atoms are situated above and below the paper plane (white and grey spheres in Fig. 3(a) respectively). Although the pyramids are arranged as in the $BaAl_4$ structure, they do not have common edges but are linked by additional bonds. When only considering the short distances in the partial structure, the layers consist of six- and four-membered rings in the ratio 2:1. The linkage of these two-dimensional (2D) nets is made by bonds between basal atoms located on top of each other (Fig. 3(b)).

$SrAl_2$ [17] crystallizes in the $CeCu_2$ structure type. The Al atoms form slightly puckered six-ring nets with almost identical bond lengths (Fig. 4(a)). Longer bonds

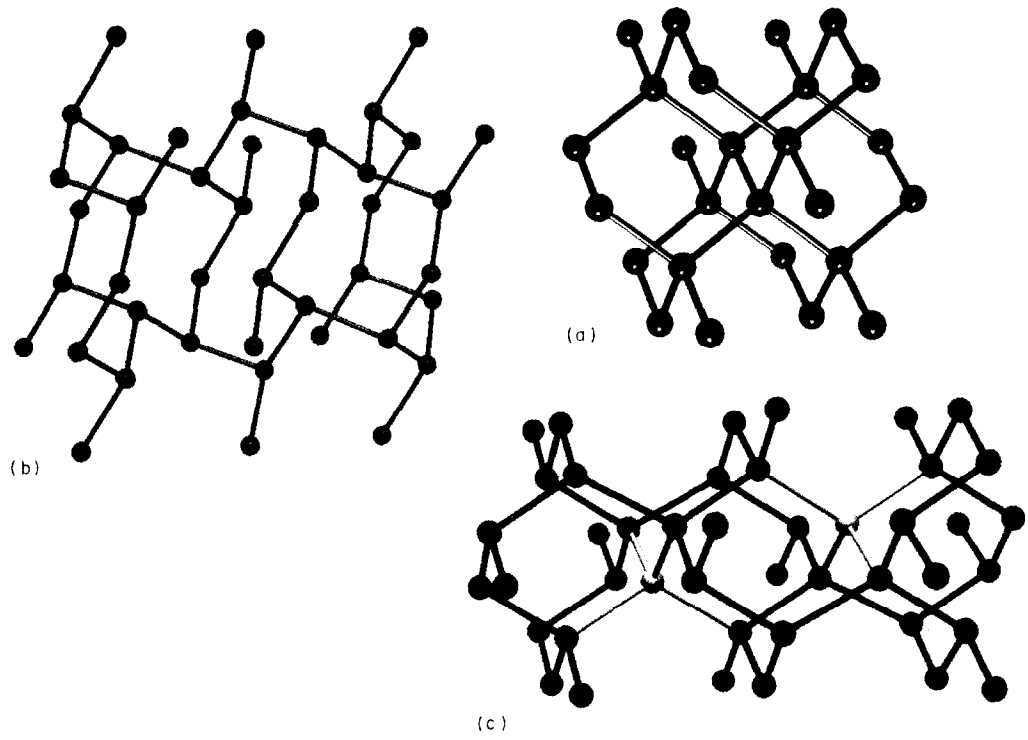

Fig. 5. (a) The diamond structure. (b) The Ga network in the MgGa structure. (c) The Ga network in the MgGa structure as a defect variant of the diamond structure. Upon putting atoms (grey spheres) in the voids of the Ga substructure in MgGa (black), the diamond structure emerges.

connect these nets, leading to zigzag chains of four membered rings. All the Al atoms have slightly distorted trigonal pyramids as coordination polyhedra.

In the Ga substructure of Ca_3Ga_5 [18] one can find 2D pieces of the Al substructure of $SrAl_2$. These stair-like pieces are built alternately of zigzag chains of four-membered rings and chains of six-membered rings (black part of the structure in Fig. 4(b)). The 2D units are linked via two-bonded Ga atoms.

LiGa [19] crystallizes in the NaTl structure type, in which the Ga atoms form the diamond structure (Fig. 5(a)).

The Ga substructure in MgGa [20] is shown in Fig. 5(b). All Ga atoms are three coordinated and form puckered eight-membered rings which are linked to a 3D network. Upon putting an additional atom in the middle of such an eight-membered ring (light spheres in Fig. 5(c)), the diamond structure appears (Fig. 5(a)). Therefore this Ga substructure can be regarded as a defect variant of the diamond structure obtained by removing one-fifth of the atoms in the diamond structure [21].

2. Calculational methods

The investigation of the structural stability of the introduced network structures has been performed within the framework of simple Hückel theory [22]. Hence one has to solve the secular determinant

$$|H_{ij}(\vec{k}) - \epsilon I| = 0 \tag{1}$$

where I is the unit matrix. The hamiltonian matrix elements are the integrals $H_{ij} = \langle \chi_i | H | \chi_j \rangle$, where χ_i is a Bloch sum of an atomic basis orbital ϕ_i located at $\vec{R}_i$:

$$\chi_i(\vec{r} - \vec{R}_i) = \sum_n \exp(i\vec{k} \cdot \vec{R}_{in}) \phi_i(\vec{r} - \vec{R}_{in}) \tag{2}$$

The summation over all unit cells n (practically truncated) and the wavevector $\vec{k}$ are consequences of the translational symmetry.

In Hückel theory the atomic orbitals ϕ_i are approximated by Slater-type orbitals (STOs). The crucial parts of the hamiltonian matrix elements are the Coulomb integrals $H_{ii} = \langle \phi_i | H | \phi_i \rangle$ and the resonance or hopping integrals $H_{ij} = \langle \phi_i | H | \phi_j \rangle$. The Coulomb integrals H_{ii} are estimated from relevant orbital ionization potentials. The resonance integrals H_{ij} are approximated by the Wolfsberg–Helmholtz formula

$$H_{ij} = \tfrac{1}{2} K S_{ij} (H_{ii} + H_{jj}) \tag{3}$$

where K is a constant. The overlap integrals $S_{ij} = \langle \phi_i | \phi_j \rangle$ have been calculated explicitly for this formula.

All calculations have been performed with atomic parameters of Ga, namely $\zeta_{4s} = 1.77$ and $\zeta_{4p} = 1.55$ for the STO exponents and $H_{4s4s} = -14.58$ eV and $H_{4p4p} = -6.75$ eV for the orbital energies.

In order to calculate relative stabilities of different structures, we followed the argumentation of Pettifor [23] by dividing the total energy per atom of any system with only one type of atom into a repulsive and an attractive part:

$$E^{\text{tot}} = E^{\text{rep}} + E^{\text{band}} \tag{4}$$

The attractive contribution is called the band energy E^{band} and is a function of the Fermi energy ϵ_F:

$$E^{\text{band}}(\epsilon_F) = \int_{-\infty}^{\epsilon_F} \epsilon n(\epsilon)\, d\epsilon \tag{5}$$

where $n(\epsilon)$ is the density of states per atom of the system.

The Hückel hamiltonian does not contain any repulsive term and so E^{rep} is not included in the solution of Eq. (1). A missing repulsive part in Eq. (4) can lead to wrong predictions when comparing structural alternatives, because E^{band} favours in general structures with higher coordination numbers [24]. In order to cope with this coordination number problem, a repulsive part is subsequently added to the total energy. E^{rep} is assumed to have pairwise character [25], namely

$$E^{\text{rep}} = \frac{1}{N_{\text{atom}}} \sum_{i<j} \varphi(\vec{R}_i - \vec{R}_j) \tag{6}$$

which also means that E^{rep} is proportional to the coordination number of atoms in the system. A reasonable estimate for the pairwise repulsive potential in sp-bonded systems is a quantity proportional to the sum of all resonance integrals between two centres $\vec{R}_i$ and $\vec{R}_j$ [25,26]:

$$\varphi(\vec{R}_i - \vec{R}_j) \propto \sum_{l,m} H_{iljm}{}^2 \tag{7}$$

The structural energy difference theorem of Pettifor [23] states that the energy difference between any two structural alternatives is approximately

$$\Delta E^{\text{tot}} \approx \Delta E^{\text{band}}|_{\Delta E^{\text{rep}}=0} \tag{8}$$

An elegant way of satisfying the constraint $\Delta E^{\text{rep}} = 0$ in (8) is provided by the moments of the density of states [8]. The calculation of the second moment μ_2 yields a quantity proportional to E^{rep} owing to the relation $\mu_2 = \Sigma_{i,j} H_{ij}{}^2$ (see Eq. (13)). The definition of the nth moment is

$$\mu_n = \int_{-\infty}^{\infty} \epsilon^n n(\epsilon)\, d\epsilon \tag{9}$$

with $n = 2$ for μ_2. Therefore the constraint $\Delta\mu_2 = 0$ is identical with $\Delta E^{\text{rep}} = 0$, where μ_2 is very easily calculated by applying the definition (9). The relation between μ_2 and E^{rep} is demonstrated in Fig. 6. It shows the calculated second moments for the Ga networks of a number of compounds as a function of the coordination number. The coordination number is the mean coordination number of the network, calculated as the mean value of the coordination numbers of all different crystallographic sites in the network. These individual coordination numbers are the effective coordination numbers (ECoNs) defined by Hoppe [27] and calculated with the assumption that all atoms in the network have the same size. The second moment varies almost linearly with the network coordination number in agreement with Eq. (6).

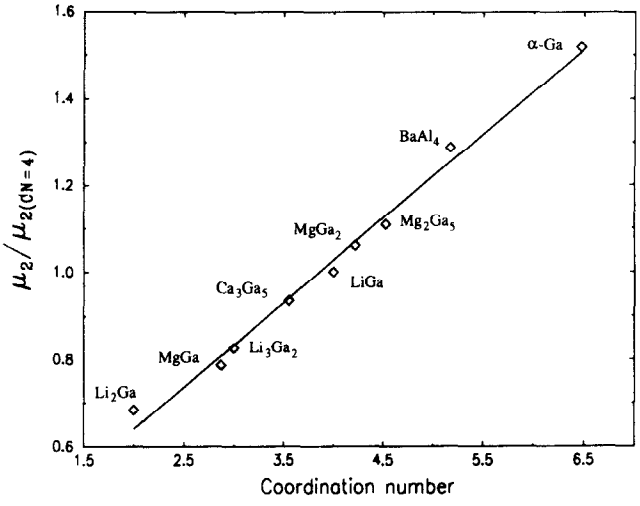

Fig. 6. The second moment of Ga network structures as a function of ECoN [27]. μ_2 has been normalized to the diamond structure formed by Ga in LiGa (ECoN = 4). The Ga substructures of Li_3Ga_2 and Li_2Ga are also taken into account. Ga atoms form in Li_3Ga_2 layers of six-membered puckered rings and in Li_2Ga planar zigzag chains.

A practical way to achieve equality of the second moments between two structures is to change the equilibrium volume of one structure (and thus the H_{ij} in Eq. (3)) until the second moments are the same. This scaling of the overall density affects only bond lengths and leaves all angles unchanged. Lee and coworkers have introduced the expression "second-moment scaling" for this procedure and show in a series of publications its wide range of use [10,28]. To study the structural energy difference ΔE^{tot} as a function of band filling or VEC, one has to reformulate Eq. (6) for E^{band}. Then the formula for the energy difference takes the form

$$\Delta E^{\text{tot}}(N) \approx \Delta E^{\text{band}}(N)|_{\mu_2-0} = \int_{-\infty}^{N^{-1}(\epsilon_{F_1})} \epsilon n_1(\epsilon)\, d\epsilon - \int_{-\infty}^{N^{-1}(\epsilon_{F_2})} \epsilon n_2(\epsilon)\, d\epsilon \tag{10}$$

where

$$N(\epsilon_F) = 2\int_{-\infty}^{\epsilon_F} n(\epsilon)\, d\epsilon \tag{11}$$

is the number of electrons per atom as a function of the Fermi energy. Index 1 refers to a reference structure with its equilibrium volume. The volume of structure 2 has been adjusted so that structure 2 has the same second moment and thus the same repulsive energy as the reference structure 1. The choice of a reference structure is arbitrary, which leads to reference-structure-dependent results when comparing the structural stability of more than two structures. In order to overcome this drawback, the simple cubic (s.c.) structure has been chosen as a neutral reference for all network structures. The peculiarity of the s.c. structure is that its density of states exhibits only little structuring, i.e. no gaps or pseudogaps occurring in $n(\epsilon)$ of structures with strong bonds or a long tail towards low energies, indicating a prevalence of three-membered rings. This ensures an almost equal influence on the various energy difference curves and therefore a good comparability between them.

In practice, μ_2 values of the Ga networks occurring in the structures of α-Ga, $SrGa_4$, Mg_2Ga_5, $MgGa_2$, LiGa, Ca_3Ga_5 and MgGa have been calculated and the mean value has been taken as the quantity proportional to a mean E^{rep} for all structures. In the next step the volumes of all networks – now including the s.c. and h.c.p. structures as well as the E13 substructure of $SrAl_2$ – have been adjusted in order to match this mean second moment. In the third step the calculation of the energy differences as a function of the number of valence electrons per E13 atom in the network structures has been performed according to Eq. (10) with the s.c. structure as reference.

Four examples of idealized energy difference curves describing the energetic difference between a structure and a reference structure as a function of the band filling are shown in Fig. 7. As a convention, the reference structure – represented as the zero line – is the more stable one of two structures for negative energy differences.

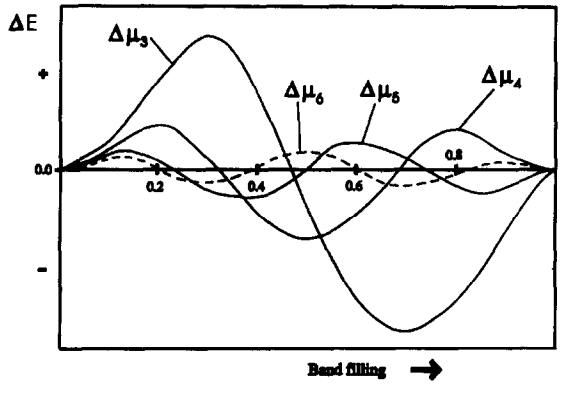

Fig. 7. Energy difference curves for structures differing only in one particular moment μ_n of the density of states from a reference structure. For positive values the structure with the larger $|\mu_n|$ is more stable. (Reproduced with permission from Ref. [6].)

The behaviour of the energy difference curves can be interpreted in terms of the moments of the density of states. These moments play an important role in an alternative to Eq. (1) for the calculation of the density of states [29]. In this context $n(\epsilon)$ is represented in the form of a continued fraction

$$n(\epsilon) = -\frac{1}{\pi}\,\mathrm{Im}\left(\cfrac{a_0}{\epsilon+b_0-\cfrac{a_1}{\epsilon+b_1-\cfrac{a_2}{\epsilon+b_2-t(\epsilon)}}}\right) \qquad (12)$$

where $t(\epsilon)$ is a function of ϵ as well as the edges of $n(\epsilon)$ and terminating $n(\epsilon)$ in Eq. (12) at the second level. The exact calculation of $n(\epsilon)$ requires many levels in the fraction, but the shapes of energy difference curves are usually determined by two or three levels [6]. The moment defined in Eq. (9) can be used for calculating the coefficients a_n and b_n, where a_n requires the knowledge of μ_0–μ_{2n} and b_n that of μ_1–μ_{2n+1} [30]. The TB Hückel hamiltonian implies the important relation [31]

$$\mu_n = \mathrm{TrH}^n = \sum_{i_1, i_2, \ldots, i_n} H_{i_1 i_2} \ldots H_{i_1 i_n} \qquad (13)$$

Eq. (13) states that the nth moment can be expressed in different paths, starting off at orbital i_1 and returning in n steps back to this orbital, each step being weighted with the appropriate integral $H_{i_l i_m}$. This geometrical meaning also has chemical importance when expressing the moments with respect to a particular site rather than an orbital: the first moment represents only the atom (summation over the Coulomb integrals), the second moment includes together with the third moment the nearest-neighbour interactions and the fourth moment also carries information about the second-nearest-neighbour interactions, etc. μ_0 is normalized to 1. In going from the first to higher moments step by step, information about interactions between a centre and its environment at an increasing distance from it is successively achieved. The energy difference theorem requires that μ_0–μ_2 are structure invariants. Thus the first and most important disparative moments are μ_3 and μ_4 and the contributions to these moments with respect to atoms are shown in Fig. 8.

The first few disparative moments control the oscillatory behaviour of the energy differences curves (see Fig. 7 for further discussion). When two structures differ only in μ_3, three nodes appear in their energy difference curve and the structure with the larger $|\mu_3|$ is the more stable at less than a half-filled band. Structures which are only different in μ_4 show four nodes in the energy difference curve, where now the structure with the smaller fourth moment is maximally stabilized for a half-filled band. The absolute differences

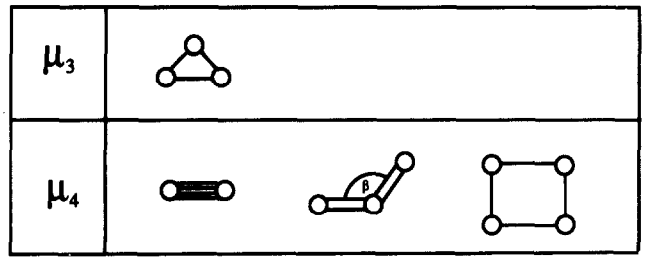

Fig. 8. Contributions of local atomic arrangements to the third and fourth moments. Each line represents all possible resonance integrals between two atoms.

in energy are much smaller in this case than for two structures differing in μ_3. In conclusion, the number of nodes of an energy difference curve usually corresponds to the level n of the first disparative moment and the amplitude of ΔE decreases rapidly as n increases.

For an interpretation of energy difference curves it is often sufficient to look at the differences in the third and fourth moments of the structures. These differences originate in the local structural features, namely in the number of three- and four-membered rings and the bond angles (Fig. 8).

In particular, a large number of three-membered rings in a structure will have the effect of a large $|\mu_3|$. The form of the triangle is also of some importance. This has been studied on a zigzag chain of Ga atoms, where μ_3 has been calculated as a function of the bond angle with the constraint $\Delta\mu_2 = 0$. Only resonance integrals between atoms of an isosceles triangle have been taken into account (see inset in Fig. 9(a)) and Fig. 9(a) shows the result: $|\mu_3|$ has a maximum for this system when the bond angle is around 70°, i.e. when the triangles are almost equilateral.

μ_4 is not only dependent on the number of four-membered rings in a structure but is also very sensitive to changes in the bond angles – the zigzag chain has again been used as a model system for investigating this influence. Only those resonance integrals of the chain have been considered which form bonds, so that a variation in the bond angle does not affect μ_2. The results depend strongly upon the chosen bond length, because bonds represent a direct contribution to μ_4. This contribution is also included in the calculation of μ_4 of the zigzag chain. Both effects are summarized in Fig. 9(b). Calculations have been performed with four different bond lengths. These bond lengths are in accordance with mean bond lengths in networks with coordination numbers (CNs) of about 12, 7, 4 and 3. First μ_4 increases strongly as the bond angle decreases. The increase in μ_4 with decreasing CN is due to the decrease in the bond lengths of the structures when going to smaller CN according to the structural energy difference theorem. This corresponds to a normalization of μ_4 to CN.

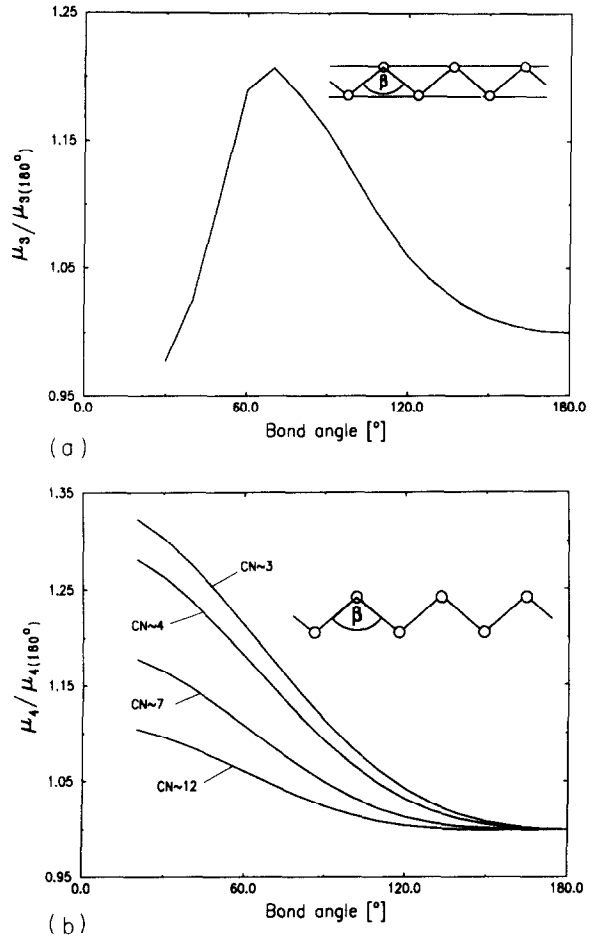

Fig. 9. (a) The angle-dependent third-moment contribution of a triangle. The calculations have been performed with the linear zigzag chain as a model system. The inset shows the model system, where the drawn lines indicate the resonance integrals which have been taken into account. The values have been normalized to μ_3 for a bond angle of 180°. (b) The two-atom fourth-moment contribution and the angle-dependent three-atom fourth-moment contribution. The different bond lengths correspond to different coordination numbers. The inset shows the model system, where the drawn lines indicate the resonance integrals which have been taken into account. The values have been normalized to μ_4 for a bond angle of 180°.

3. Structural trends and their origin

Figs. 10(a) and 10(b) summarize the calculated energy difference curves with respect to the s.c. structure as reference. The great number of four-membered rings in the s.c. structure has the effect of a large μ_4 and, because a square represents two rectangular triangles, $|\mu_3|$ is also quite large. The shape of the curves can be thought as a superposition of the idealized energy difference curves in Fig. 7 with three and four nodes for structures differing in μ_3 and μ_4. The alteration of $\Delta\mu_3$ with the increase in VEC determines the rough shape of the curves. Only the h.c.p. structure has a larger $|\mu_3|$ than the s.c. structure. It is the most stable structure until the valence electron concentration exceeds two electrons per atom. Then the α-Ga structure

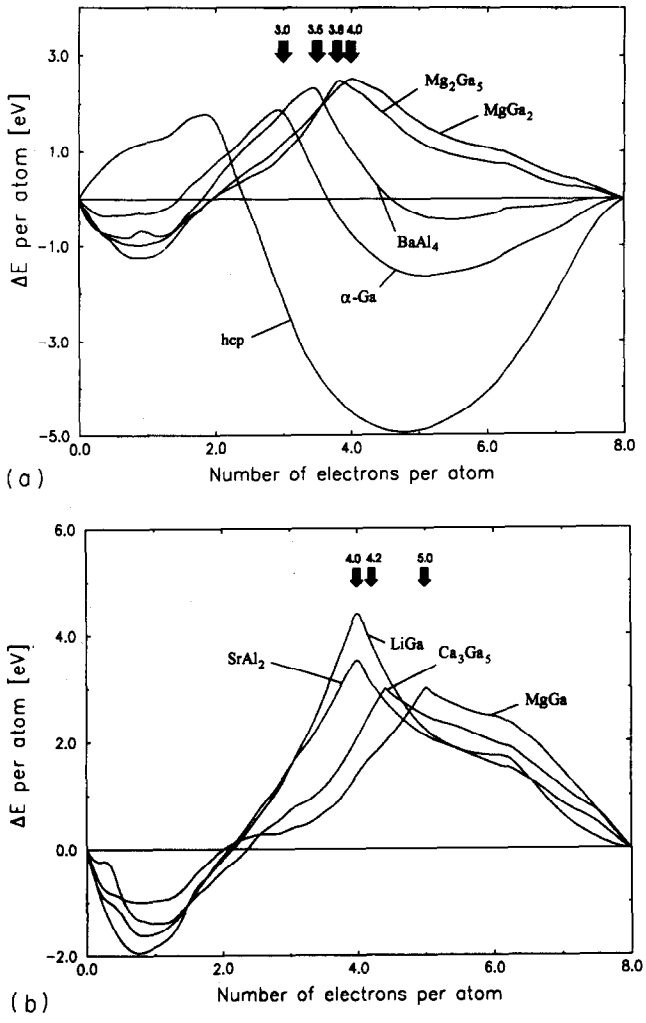

Fig. 10. (a) Energy difference curves between electron-deficient network structures and the s.c. structure as reference. (b) Energy difference curves between valency network structures and the s.c. structure as reference. The VECs corresponding to the composition of the intermetallic. Compounds are marked with arrows.

becomes more stable. The values of $|\mu_3|$ for the α-Ga structure, the substructure of $BaAl_4$ and the s.c. structure are about the same, because the energy difference curves are controlled by a difference in μ_4 and thus exhibit four nodes. The shape of all other energy difference curves is determined by the larger $|\mu_3|$ of the s.c. structure but is also considerably modulated by a $\Delta\mu_4$ curve, where the reference structure always has the larger μ_4.

The curves of the substructures of the binary compounds have their maxima at a valence electron concentration corresponding to complete electron transfer from the electropositive component to the more electronegative substructure, which is in the spirit of the Zintl–Klemm concept. This can be interpreted such that the electrons occupy essentially states which contribute to the bonding of the E13 partial structure. The only exception is Ca_3Ga_5, which has its maximum at VEC=4.4 instead of 4.2.

The most important moments μ_3 and μ_4 as a function of the ECoN of the substructures are illustrated in Fig. 11. On going from h.c.p. (ECoN=12, not drawn) to the substructure of $MgGa_2$ (ECoN=4.22), $|\mu_3|$ and μ_4 decrease constantly. The networks in this range are usually denoted as electron deficient. However, as in deltahedral clusters, electron deficiency is more a terminus of classification and not an actual state, because all the networks have their stability maximum at the observed VECs. At ECoN=4 a discontinuity in the course of $|\mu_3|$ and especially μ_4 occurs. This corresponds to the transition from electron-deficient structures to valency compounds, which is accompanied by the opening of a broad band gap at the Fermi level. Towards lower ECoN $|\mu_3|$ and μ_4 increase again, with μ_4 showing the greater variations.

In order to examine the significance of μ_3 and μ_4 to the energy difference curves, $n(\epsilon)$ has been calculated to the second level according to Eq. (12). Therefore knowledge of μ_0–μ_5 was required. Termination has been performed with the square root terminator [32], which leads to a continuous $n(\epsilon)$. The values of the band edges have been taken from the previous $\vec{k}$-dependent calculations (Eq. (1)). The result is shown in Figs. 12(a) and 12(b) and can be directly compared with Figs. 10(a) and 10(b). Knowledge of the first few moments together with the edges of $n(\epsilon)$ is sufficient to approximate the overall shape and the amplitudes of the exact energy difference curves remarkably well. Only the very closely lying curves of the networks of Mg_2Ga_5 and $MgGa_2$ are not separated sufficiently. The maxima, however, are not reproduced exactly until $n(\epsilon)$ is calculated to eight levels. This means that the fine structure of $n(\epsilon)$ is crucial for the correct maxima and therefore knowledge of very high moments is required.

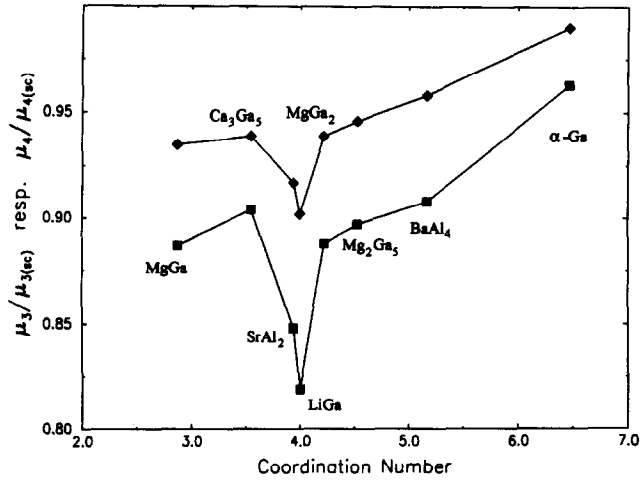

Fig. 11. The third moments (upper curve) and the fourth moments (lower curve) of the investigated network structures as a function of their ECoN [27]. The values of the moments have been normalised to that of the sc reference structure. The values for the hcp structure (not drawn) are $\mu_3/\mu_{3(sc)}=1.082$ and $\mu_4/\mu_{4(sc)}=1.133$.

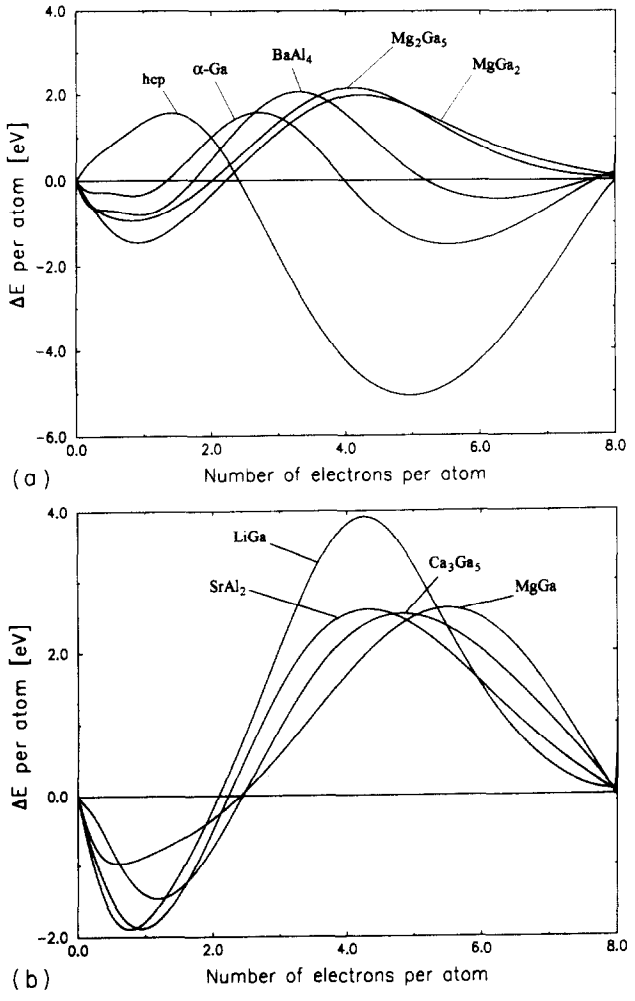

Fig. 12. Energy difference curves from calculations based on the recursion method (Eq. 12, [29]). The only structure dependent information used for the calculations are the knowledge of μ_3 to μ_5 and the edges of $n(\epsilon)$ of a particular structure. In (a) the difference curves between electron-deficient network structures and the sc structure as reference and in (b) the difference curves between valency network structures and the sc structure as reference are shown.

When comparing the stability ranges of different substructures, one has to be aware that they are stabilized additionally by the interaction with the positively polarized alkali or alkali earth components. These Madelung contributions should basically affect the amplitude and not the electronically controlled shape of the energy difference curves of the investigated E13-rich binary compounds. For example, the diamond structure formed by Ga atoms in LiGa conceals all other structural alternatives for a VEC around four electrons per atom. The size of the cationic component also has a contribution to the determination of a particular substructure, thus leading to the diversity of substructures in binary compounds with the same stoichiometry. This indicates clearly that the VEC is not the only variable when investigating absolute structural stabilities [33].

The interplay of μ_3 and μ_4, determining the ranges of stability as a function of the valence electron concentration, has its origin in the local atomic environments. The h.c.p. structure is dominated by the great number of equilateral triangles leading to a large $|\mu_3|$, which stabilizes this structure at low valence electron concentrations. Going to the α-Ga structure, the significant triangles occur only in the 2D puckered layers (Fig. 1(b)). The stacking of these layers via the short bonds induces skew hexagons with considerably larger bond angles (see Fig. 9(a)). The net effect is a reduction of $|\mu_3|$ and therefore a maximal stabilization at three electrons per atom. On a molecular level this trend can be estimated even from three atom arrangements, namely the closed and the open three-centre bonds (Scheme 1), where suitable electron counts are two and four respectively. This trend is continued in the substructure of $BaAl_4$. The 2D layers of pyramids (Fig. 2(a)) consist of even fewer triangles. The stacking of the layers is accompanied by the formation of hexagons analogous to the α-Ga structure. Starting from the substructure of $BaAl_4$, two possibilities are realized to reduce $|\mu_3|$ further. In the substructure of $MgGa_2$, triangle containing chains of top-connected pyramids are linked via hexagons. The linkage of these strands raises the number of hexagons considerably compared with the situation in the network of the $BaAl_4$ structure.

Another possibility is to dilute the number of pyramids in the 2D layers of the $BaAl_4$ structure. This is found in the network of the Mg_2Ga_5 structure, where the condensed pyramids of the $BaAl_4$ structure are separated and linked by additional bonds (Fig. 3(a)). Thus additional hexagons inside the 2D layers are introduced besides those which result from the stacking of the layers. In conclusion, triangles are no longer the predominant structural feature for these two networks. The reduction of $|\mu_3|$ and μ_4 is caused by an overall increase in the bond angles. Therefore more and more

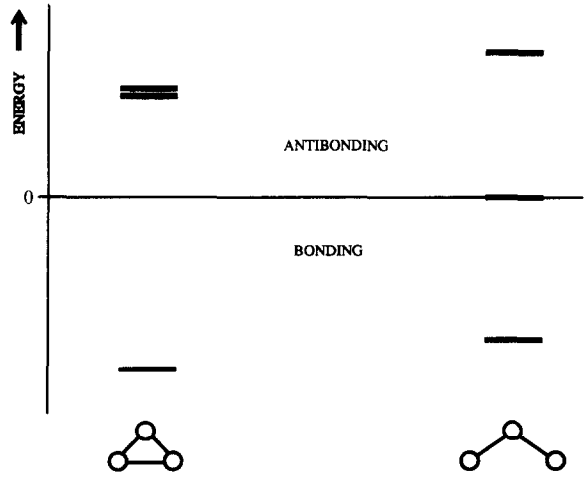

Scheme 1.

six-membered rings appear in the structures which are stable at higher VEC. Additionally, μ_4 is influenced by the presence of four-membered rings in the networks of the $BaAl_4$, Mg_2Ga_5 and $MgGa_2$ structures. Thus the interplay of three-, four- and six-membered rings controls the structural stability of the electron-deficient networks.

In the diamond structure (Ga substructure of LiGa) the hexagons remain as the only structural feature. Bond angles around 110° lead to a very small μ_4 which stabilizes a structure at exactly half-full bands. Considering the substructure of MgGa as a defect variant of the diamond structure, the decrease in μ_4, which shifts the stability maximum to a VEC of five electrons per E13 atom, is mainly due to the reduction of the bond lengths.

The E13 atoms in $SrAl_2$ are formally four bonded. However, a closer look at the chemical bonding in this substructure suggests a π bonding contribution within the puckered six-ring layers [34]. This structure may also be regarded as an intermediate between the BN and the hexagonal diamond structure (londsdaleite) and the coordination of the E13 atoms proposes hybridization between sp^2 and sp^3. The optimal VEC is four electrons per E13 atom (Fig. 10(b)). This curious coordination is not exceptional in intermetallic networks; it occurs again in the substructure of Ca_3Ga_5, which consists of 2D pieces of the $SrAl_2$ substructure. The 2D units are connected by two-bonded E13 atoms and the insertion of these bridging atoms is responsible for the rise of μ_4 and therefore the stabilization at higher VEC. The observation that higher VECs in electron-deficient networks are often adapted by a dilution of structural units typical of lower VEC also holds for the valency compounds, especially the Zintl phases.

4. Conclusions

The simple TB Hückel theory in conjunction with the structural energy difference theorem has proved to be a successful method for studying the electronically driven changes in the network structures formed by gallium and aluminium. The networks occur in the elemental structures and especially in intermetallic compounds and can be divided into electron-deficient (VEC $\leqslant$ 4) and valency (VEC $\geqslant$ 4) structures.

The maxima of the calculated energy difference curves agree, with one exception, with the VECs if one assumes complete electron transfer from the electropositive components to the network substructures on the basis of the observed compositions of the intermetallic compounds.

The absolute prediction of VEC-dependent stability ranges suffers a bit from the non-comparability of the amplitudes of the energy difference curves because of neglected interactions with the electropositive components.

The method of moments can explain qualitatively the observed stability trends. In close-packed structures equilateral triangles are the only structural feature. The resulting large $|\mu_3|$ values stabilize such structures at low VEC. With increasing VEC the electron-deficient network structures react with the dilution of triangle-containing structural units in various ways in order to decrease $|\mu_3|$ until the valency network structures become stable (VEC $\geqslant$ 4). These structures are first dominated by hexagons which stabilize a structure at half-filled bands through the small μ_4. A further increase in VEC leads to a dilution of the hexagon-containing structural units in order to increase μ_4. The contributions of structural features to the moments of the density of states are very often interrelated, which makes it difficult to attribute a specific structural change to the change in one particular moment.

The wider application of this method to intermetallic networks [35] seems to be attractive. Very often it is difficult to identify the important building blocks in such structures, especially in those containing transition elements. The investigation of the electronic significance of nets in intermetallic compounds could help to extract reasonable building blocks for a more general understanding of their structures. We feel that this concept can help to screen out the important substructures from the large number of connectivities in intermetallic phases.

References

[1] C. Belin and M. Tillard-Charbonnel, *Prog. Solid State Chem., 22* (1993) 59.

[2] S.C. Sevov and J.D. Corbett, *Inorg. Chem., 30* (1991) 4875; *J. Solid State Chem., 103* (1993) 114.
Z. Dong and J.D. Corbett, *J. Am. Chem. Soc., 115* (1993) 11 299.

[3] W. Blase, G. Cordier and M. Somer, *Z. Kristallogr., 194* (1991) 150.
G. Cordier and V. Müller, *Z. Kristallogr., 198* (1992) 281.

[4] J.K. Burdett and E. Canadell, *J. Am. Chem. Soc., 112* (1990) 7207; *Inorg. Chem., 30* (1991) 1991.

[5] K. Wade, *Adv. Inorg. Chem. Radiochem., 18* (1976) 1.

[6] J.K. Burdett and S. Lee, *J. Am. Chem. Soc., 107* (1985) 3050.

[7] W.B. Pearson, *J. Less-Common Met., 109* (1985) L7.

[8] F. Ducastelle and F. Cyrot-Lackmann, *J. Phys. Chem. Solids, 32* (1971) 285.

[9] A.J. Bradley, *Z. Kristallogr., 91* (1935) 302.

[10] S. Lee, R. Rousseau and C. Wells, *Phys. Rev. B, 46* (1992) 12 121.

[11] H.G. von Schnering and R. Nesper, *Acta Chem. Scand., 45* (1991) 870.

[12] X.G. Gong, G.L. Chiarotti, M. Parinello and E. Tosatti, *Phys. Rev. B, 43* (1992) 14 277.

[13] K.R. Andress and E. Alberti, *Z. Metallkd., 27* (1935) 126.

[14] C. Zheng and R. Hoffmann, *Z. Naturf. B, 41* (1986) 292.
J.K. Burdett and G.J. Miller, *Chem. Mater., 2* (1990) 12.

[15] G.S. Smith, K.F. Mucker, Q. Johnson and D.H. Wood, *Acta Crystallogr. B, 25* (1969) 549.
[16] G.S. Smith, Q. Johnson and D.H. Wood, *Acta Crystallogr. B, 25* (1969) 554.
[17] G. Nagorsen, H. Posch, H. Schäfer and A. Weiss, *Z. Naturf. B, 24* (1969) 1191.
[18] G. Cordier, H. Schäfer and M. Stelter, *Z. Anorg. Allg. Chem., 539* (1986) 33.
[19] E. Zintl and G. Brauer, *Z. Phys. Chem. B, 20* (1933) 245.
[20] K. Schubert, F. Gauzzi and K. Frank, *Z. Metallkd., 54* (1963) 422.
[21] A. Grüttner, *Thesis*, University of Stuttgart, 1982.
[22] M.-H. Wangbo, M. Evain, T. Hughbanks, M. Kertesz, S. Wijeyesekera, C. Wilker, C. Zheng and R. Hoffmann, *Program* EHMACC: *Extended Hückel Molecular and Crystal Calculations; Program* EHPC: *Extended Hückel Property Calculations.*
[23] D.G. Pettifor, *J. Phys. C: Solid State Phys., 19* (1986) 285.
[24] J.K. Burdett, *Struct. Bond., 65* (1987) 86.
[25] D.G. Pettifor and R. Podloucky, *J. Phys. C: Solid State Phys., 19* (1986) 315.
[26] J.C. Cressoni and D.G. Pettifor, *J. Phys.: Condens. Matter, 3* (1991) 495.
[27] R. Hoppe, *Angew. Chem. Int. Edn. Engl., 9* (1970) 25; *Z. Kristallogr., 150* (1979) 23.
[28] S. Lee, *Acc. Chem. Res., 24* (1991) 249; *J. Am. Chem. Soc., 113* (1991) 101.
L.M. Hoistad and S. Lee, *J. Am. Chem. Soc., 113* (1991) 8216.
L.M. Hoistad, S. Lee and J. Pasternak, *J. Am. Chem. Soc., 114* (1992) 4790.
[29] R. Haydock, in F. Seitz, D. Turnbull and H. Ehrenreich (eds.), *Solid State Physics,* Vol. 35, Academic, New York, 1980, p. 215.
[30] J.P. Gaspard and P. Lambin, in D.G. Pettifor and D.L. Weaire (eds.), *Springer Series in Solid State Sciences,* Vol. 58, *The Recursion Method and Its Application,* Springer, Berlin, 1985, p. 72.
[31] F. Cyrot-Lackmann, *J. Phys. Chem. Solids, 29* (1986) 1235.
[32] M.J. Kelly, in F. Seitz, D. Turnbull and H. Ehrenreich (eds.), *Solid State Physics,* Vol. 35, Academic, New York, 1980, p. 314.
[33] P. Villars, K. Mathis and F. Hulliger, in F.R. de Boer and D.G. Pettifor (eds.), *The Structure of Binary Compounds,* Elsevier, New York, 1989, p. 1.
[34] U. Häußermann, S. Wengert and R. Nesper, *Angew. Chem. 106* (1994) 2150; *Angew. Chem. Int. Edn. Engl., 33* (1994) 2073.
[35] W.B. Pearson, *The Crystal Chemistry and Physics of Metals and Alloys,* Wiley, New York, 1972.